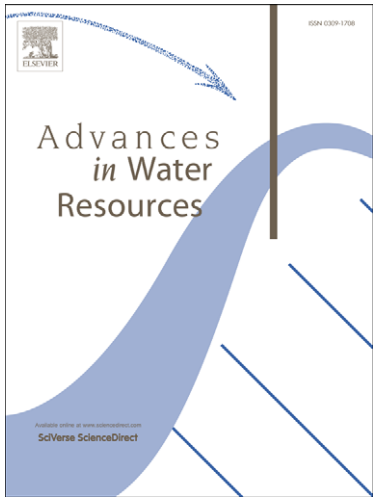

Modeling Bimolecular Reactions and Transport in Porous Media Via Particle Tracking

Dong Ding, David A. Benson, Amir Paster, Diogo Bolster

PII: S0309-1708(12)00276-X
DOI: http://dx.doi.org/10.1016/j.advwatres.2012.11.001
Reference: ADWR 1971

To appear in: *Advances in Water Resources*

Received Date: 31 May 2012
Revised Date: 30 October 2012
Accepted Date: 2 November 2012

Please cite this article as: Ding, D., Benson, D.A., Paster, A., Bolster, D., Modeling Bimolecular Reactions and Transport in Porous Media Via Particle Tracking, *Advances in Water Resources* (2012), doi: http://dx.doi.org/10.1016/j.advwatres.2012.11.001

Modeling Bimolecular Reactions and Transport in Porous Media Via Particle Tracking

Dong Ding

Hydrologic Science and Engineering, Colorado School of Mines, Golden, CO, 80401, USA. (dding@mines.edu)

David A. Benson

Hydrologic Science and Engineering, Colorado School of Mines, Golden, CO, 80401, USA. (dbenson@mines.edu)

Amir Paster

Environmental Fluid Mechanics Laboratories, Dept. of Civil Engineering and Geological Sciences, University of Notre Dame, Notre Dame, IN, USA

Diogo Bolster

Environmental Fluid Mechanics Laboratories, Dept. of Civil Engineering and Geological Sciences, University of Notre Dame, Notre Dame, IN, USA

Abstract

We use a particle-tracking method to simulate several one-dimensional bimolecular reactive transport experiments. In our numerical scheme, the reactants are represented by particles: advection and dispersion dominate the flow, and molecular diffusion dictates, in large part, the reactions. The particle/particle reactions are determined by a combination of two probabilities dictated by the physics of transport and energetics of reaction. The first is that reactant particles occupy the same volume over a short time interval. The second is the conditional probability that two collocated particles favorably transform into a reaction. The first probability is a direct physical representation of the degree of mixing in an advancing interface between dissimilar waters, and as such lacks empirical parameters except for the user-defined number of particles. This number can be determined analytically from concentration autocovariance, if this type of data is available. The simulations compare favorably to two physical experiments. In one,

the concentration of product, 1,2-naphthoquinoe-4-aminobenzene (NQAB) from reaction between 1,2-naphthoquinone-4-sulfonic acid (NQS) and aniline (AN), was measured at the outflow of a column filled with glass beads at different times. In the other, the concentration distribution of reactants ($CuSO_4$ and $EDTA^{4-}$) and product ($CuEDTA^{2-}$) were quantified by snapshots of light transmitted through a column packed with cryolite sand. These snapshots allow us to estimate concentration statistics and calculate the required number of particles. The experiments differ significantly due to a $\sim 10^7$ difference in thermodynamic rate coefficients, making the latter experiment effectively instantaneous. When compared to the solution of the advection-dispersion-reaction equation (ADRE) with the well-mixed reaction coefficient, the experiments and the particle-tracking simulations showed on the order of 20% to 40% less overall product, which is attributed to poor mixing. The poor mixing also leads to higher product concentrations on the edges of the mixing zones, which the particle model simulates more accurately than the ADRE.

Keywords: Lagrangian Particle Method, Chemical Reactions
PACS: 02.50.Ey, 02.50.Ga, 02.70.Ns, 05.10.Gg

1. Introduction

As groundwater moves through an aquifer, it often undergoes chemical reaction as it mixes with chemically dissimilar water or encounters reactive solids. The reactions are local phenomena, but predictions of reactive transport are often made at much larger scales. This mismatch of scales has been found to degrade the predictions of reaction. In particular, the reaction rates at the larger scale are found be be much less than those measured in the laboratory [1, 2, 3, 4]. To make predictions, a Fickian transport equation is typically coupled to a chemical reaction equation to form the advection-dispersion-reaction equation (ADRE):

$$\partial C_i/\partial t = -\nabla \cdot (\mathbf{u} C_i - D \nabla C_i) - r_i \tag{1}$$

where $C_i(\boldsymbol{x}, t)$ is the concentration, t is time, $\mathbf{u}(\boldsymbol{x}, t)$ is the Darcy scale pore water velocity, $D(\boldsymbol{x}, t)$ is the hydrodynamic dispersion tensor, and $r_i(\boldsymbol{x}, t, C_1, C_2, ...)$ is the reaction rate of species i. The reaction rate, a crucial term in ADRE, is commonly estimated from batch tests under perfect

mixing conditions of the same reaction [5, 6, 4, 7, 8, 3]. When this reaction rate is used in Eq. (1) to predict miscible displacement and reaction in column- and field-scale tests, the observed reaction rate is generally much smaller [6, 9, 10, 11]. An effective reaction coefficient (< 1), is commonly applied to the last term of ADRE to account for the over-estimated reaction [12, 7, 6, 13]. Unfortunately, the coefficient value is difficult to determine and varies from case to case (and scale to scale) [6, 8].

Laboratory and numerical experiments (e.g., [8, 5, 12]) revealed that incomplete mixing is primarily responsible for the reduced reaction rates. The dispersion term in Eq. (1) simultaneously describes both spreading of, and mixing among, solute fronts between dissimilar water. But in real-world and synthetic tests, the spreading rate is found to be greater than the mixing rate [14, 11, 15, 16, 17, 18, 19]; therefore, an equation that correctly simulates spreading will overpredict the mixing of the water. For example, *Kapoor et al.* [8] theorized (and showed numerically) that the simple bimolecular reaction ($A + B \rightarrow C$) for Poiseuille flow and Taylor dispersion within a single tube would result in reduced reaction relative to the well-mixed rate. In a series of numerical and laboratory experiments, *Raje and Kapoor* [5] constructed a glass bead-filled column and showed that the product concentration in the column was approximately 40% less than what was predicted by Eq. (1) in one-dimension ($1D$). *Gramling et al.* [12] found overall product production of approximately 20% less in their column than predicted by Eq. (1) based on experiments at different flow velocities. These observations point to several deficiencies of the ADRE: i) the deterministic concentration neglects small-scale fluctuations [5, 12, 7, 20]; ii) the reactants are assumed to be well-mixed, which is unusual under natural conditions [6, 20, 21], and iii) the dispersion term is forced to account for both the spreading and the dilution, or mixing, of the species [22, 23].

The mixing that leads to reaction is often limited to transverse dispersion and diffusion. In porous media, these mechanisms are orders-of-magnitude lower than longitudinal dispersion [5, 24, 22, 14]. In recent studies, both *Edery et al.* [20] and *Tartakovsky et al.* [21] noticed that the slow diffusion of the reacting species into and out of plume boundaries determines the reaction rate and explains why averaged concentration models over-predict the amount of reaction. A variety of studies (e.g., [25, 26, 27, 28]) demonstrate that reactants are not perfectly mixed and diffusion is a limiting process even in free fluid flow without the structure imposed by porous media.

A series of theoretical studies [6, 29, 9] showed that the upscaled equations

of reaction in the presence of diffusion are different from the perfectly-mixed equation and uniquely defined by the transport mechanism, These studies showed that it not necessarily proper to arbitrarily combine transport and reaction equations. Various reactive transport models have been proposed [30, 31, 32, 10, 33, 4, 21, 34] and a variety of laboratory (e.g.,[5, 12, 35]) and field studies (e.g., [36, 37, 38, 39, 40]) have been conducted to test the validity of various modeling approaches that separately account for mixing, reaction, and transport. One approach is a Lagrangian particle tracking (PT) method. The general Lagrangian framework has given rise to several algorithms that represent smaller-scale physics in different ways. For example, the smoothed particle hydrodynamics method simulates a given partial differential equation (PDE) on moving particles instead of on a fixed grid [41, 42, 10]. This method rests on the assumption that the chosen PDE for transport and reaction is the correct one at some smaller scale.

A different Lagrangian model from *Benson and Meershaert* [29] makes no assumption about the form of the governing equation for reaction. Their PT method simulates chemical reactions through probabilistic rules of particle collisions, interactions, and transformations. The method is based on an explicit calculation of the probability that any two particles will be co-located in any time interval, in combined with the independent probability that two particles, upon co-location, will react. The second probability is the well-mixed reaction rate scaled appropriately by the number of particles and the volume associated with that rate. *Benson and Meerschaert's* [29] method is an extension of *Gillespie's* [43], which uses a well-mixed assumption to calculate the probability of particle co-location (and leads to the classical mass-action reaction equations [44]). It was shown recently by *Paster et al.* [45] that at the limit of infinitely small time step and infinite number of particles, the PT method converges to the well-mixed ADRE (1) using the classical law of mass action for a bimolecular reaction.

Other approaches have also been proposed, such as different forms of underlying transport [9, 46, 47], time dependent reaction rate coefficients [48, 49], stochastic perturbation models [7], and multi-rate mass transfer [50, 51]. These models can be calibrated to simulate the reactive transport successfully by reproducing anomalous flux-averaged breakthrough curves [52, 21]. However, as indicated by *Tartakovsky et al.* [21], these approaches require additional effective parameters, which can only be obtained from calibration with experimental data.

In this study, we test the hypothesis that the bulk of the experimental

observations can be explained by the application of simple, physically-based rules of transport and reaction within a Lagrangian framework. The transport algorithm is based on Fickian dispersion with a mean advective drift, and the bimolecular reactions use the PT method from *Benson and Meerschaert* [29], in which the reaction probability only depends on the thermodynamic rate of the chemical reaction and the distribution of particles in both space and time.

2. Methods

2.1. Summary of Column Experiments

We consider the column experiments conducted by *Raje and Kapoor* [5] and *Gramling et al.* [12], which are widely regarded as benchmarks of reactive transport in porous media [53, 20, 49, 46]. *Raje and Kapoor* [5] used a spectrophotometer to obtain the outflow concentrations of product from the transport and reaction of 1,2-naphthoquinone-4-sulfonic acid (NQS) and aniline (AN) in a column filled with glass beads. They ran two experiments, each with different flow rates and concentrations of reactants. *Gramling et al.* [12] took images of light transmitted through a colorimetric reaction between aqueous $CuSO_4$ and $EDTA^{4-}$ within a translucent chamber packed with cryolite sand to observe the concentration distribution of compounds within the column. They ran three experiments at three different velocities with all other parameters held constant. The physical setup of all of the experiments considered here was similar. Initially, the columns were saturated with one species at concentration C_0, and the other reactant was introduced at the inlet at a constant rate and the same constant concentration C_0. Peclet numbers of both experiments were high, but Reynolds numbers were sufficiently low to ensure laminar flow.

Before performing the column experiments, the reaction rate constants were obtained with high confidence from well-mixed batch experiments. Dispersion coefficients at each velocity were measured via conservative tracer, and diffusion coefficients were gathered from the literature. Hydrodynamic dispersion dominated over diffusion in spreading the inert tracer at all velocities. The parameters from the two experiments under different flow conditions are summarized in Table 1.

Primarily because of the different reactions rates, different solution methods were used to evaluate the experimental results in these two studies, even though both assumed one-dimensional flow. For a well-mixed system, the

law of mass action for the irreversible reaction $A + B \rightarrow P$ can be expressed as $r_A = r_B = -r_P = dC_A/dt = -k_f C_A C_B$. Both groups used this law in the ADRE (1) to compare to experimental results. *Raje and Kapoor* [5] solved the ADRE (1) at the outflow using the finite difference (FD) scheme. *Gramling et al.* [12] used an analytical solution by assuming the reaction was instantaneous and the boundaries remote. Their solution is

$$\frac{C_P}{C_0} = \frac{1}{2}\text{erfc}\left(\frac{|x - ut|}{\sqrt{2Dt}}\right), \tag{2}$$

where $C_P(x,t)$ is product concentration, and C_0 is the constant flux concentration of the injected reactant at the inlet boundary [12]. We also use an FD solution to compare to *Raje and Kapoor's* [5] data and the analytic solution (2) for *Gramling et al.'s* [12] data.

Simulation	Gramling et al.			Raje and Kapoor	
Length (cm)	30	30	30	18	18
Rate Constant ($M^{-1}s^{-1}$)	2.3×10^9	2.3×10^9	2.3×10^9	4.38×10^2	4.38×10^2
Flow Rate (mL/s)	0.0445	0.267	2.5	-	-
Pore Velocity (cm/s)	0.0121	0.0832	0.670	0.096	0.070
Dispersion Coeff. (cm^2/s)	1.75×10^{-3}	1.45×10^{-2}	1.75×10^{-1}	3.17×10^{-2}	2.31×10^{-2}
Diffusion Coeff. (cm^2/s)	7.02×10^{-7}	7.02×10^{-7}	7.02×10^{-7}	4.6×10^{-6}	4.6×10^{-6}
Concentration (M)	0.02	0.02	0.02	5.0×10^{-4}	2.5×10^{-4}

Table 1: Experimental parameters.

2.2. Methodology of Particle Reaction and Transport

Our particle tracking algorithm separately simulates transport and reactions in any given time step. For reaction, the model assumes that molecular diffusion dictates the probability that reactants can mix and react at the pore-scale. The probability density for particle co-location is calculated as $v(s) = \int f_A(x) f_B(s + x) dx$, where $f_A(x)$ and $f_B(x)$ denote the densities of the motions of A and B particles away from their current positions, and s is the initial particle separation distance [29]. For a time step of duration Δt, the Gaussian local diffusion has variance $2D_m\Delta t$, where D_m is the molecular diffusion coefficient, and the co-location density is a convolution of two of these Gaussians, which is also Gaussian but with variance $4D_m\Delta t$. For computational efficiency, *Benson and Meerschaert* [29] approximated the Gaussian with a piecewise linear "tent" function with the same variance:

$$v(s) = \max\left\{0, \frac{-|s|}{24D_m\Delta t} + (24D_m\Delta t)^{-1/2}\right\}. \tag{3}$$

The differential co-location probability $v(s)ds$ is approximated with a finite volume $v(s)\Delta s$ and combined with the thermodynamic probability to find the total probability of reaction using

$$\text{Prob}(react) = k_f \Delta t \Omega C_0 v(s)/N_0 \tag{4}$$

where k_f [$\text{M}^{-1}\text{L}^d\text{T}^{-1}$] is the reaction rate constant, Δt is the time interval, Ω [L^d] is the column size in d-dimensions, C_0 is the initial concentration of the resident (say B) species [ML^{-d}], and N_0 is the initial number of B particles [29]. The rate k_f is the rate associated with a reaction volume, taken here to be the volume associated with a particle (discussed more in section 2.3). At every time step, each A particle is selected sequentially to see if it will react. B particles that are sufficiently close are searched, and the probability of co-location is calculated, one B particle at a time. The combined probability is compared with a random number between 0 and 1. If the probability of the reaction is larger than the random number, the two particles are removed from the domain and a P particle is placed randomly between the initial A and B particle locations.

The advection-dispersion process for each particle is simulated over a time step of duration Δt using the approximate Langevin equation [15, 54, 55, 56]

$$X(t + \Delta t) = X(t) + u\Delta t + Z \cdot \sqrt{2D\Delta t}, \tag{5}$$

where $X(t)$ is the location of a particle at time t, u is the average pore water velocity, Z is a standard Normal random variable, and D is the reported dispersion coefficient. We substitute a shifted and scaled uniform [0,1] random variable $\sqrt{24D\Delta t}(U(0,1) - 1/2)$ for the last term [6, 29]. The selection of Δt is based on two criteria: i) the maximum reaction probability (Eq. (4) with $s = 0$) is less than unity to fulfill the definition of a probability, and ii) the time interval is relatively small compared to total residence time, so that a sufficient number of random motions are completed to agree with the analytical solution of (1) for r_i= 0 (Fig. 1).

The initial conditions and boundary conditions are based on the experimental setup. They can be expressed as: $C_B(x, 0) = C_0$ and $C_A(x, 0) = 0$ for $x \geq 0$ (species B occupies the domain uniformly and there is no A species initially); $C_A(0, t) = C_0$ for $t \geq 0$ (constant concentration of A species input at the upstream end); and $\partial C_{A,B}(L, t)/\partial x = 0$ for $t \geq 0$ at the column end L.

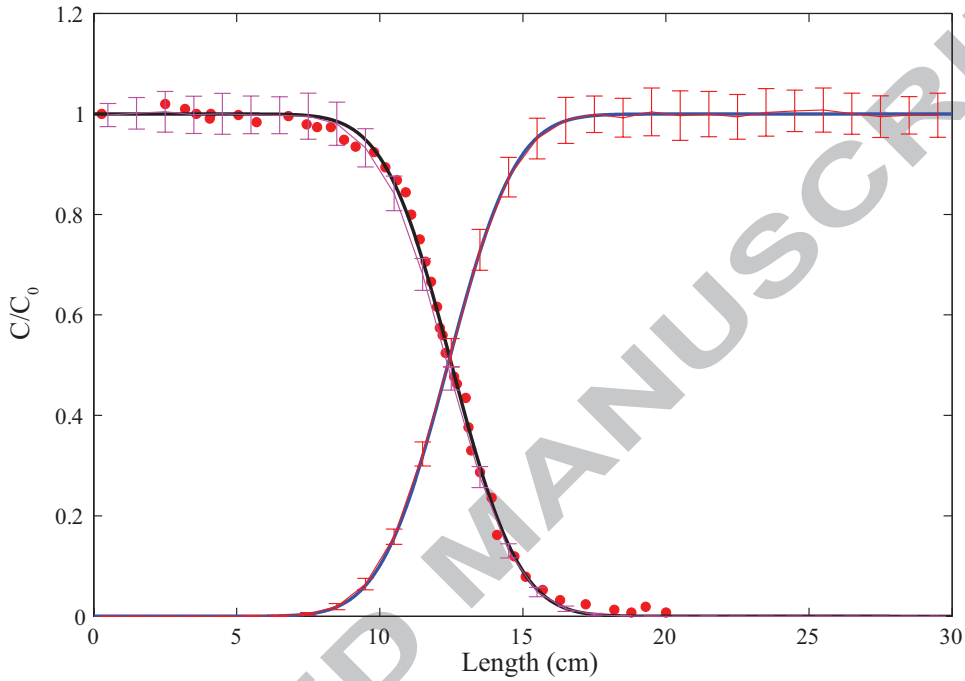

Figure 1: Verification of particle tracking for non-reactive transport. The red dots are experimental column-width averages of snapshots of $CuEDTA^{2-}$ at 1023 seconds from [12]. The blue and black solid lines are analytical solutions of the ADE for two species flowing through a column in which one species saturates the column initially, and the other enters at constant concentration from the upstream ($x = 0$) end. The red and magenta lines with error bars represent the simulations using PT method.

For every time step, the particles move in the column based on Eq. (5), and the reaction of each A particle in the domain is checked with possible B particles through Eq. (4). This process is repeated for every transport/reaction time step. Computation of the distances between every A and B particle is costly if a large number of particles are simulated. To improve efficiency, we apply the KD-tree technique of *Bentley* [57] as implemented by *Tagliasacchi* [58]. A KD-tree (short for K-dimensional) is a binary tree for efficient storage of neighbor information to be retrieved by searches [57]. The KD-tree algorithm partitions space into K-dimensional blocks with particles along edges, and maps the adjacent blocks in a tree structure so that a search can march orderly through adjacent blocks. For N particles at any time step, creating the tree takes $\mathcal{O}(N \ln N)$ operations, and each search takes $\mathcal{O}(N)$ operations so that each reaction time-step goes like $\mathcal{O}(N \ln N)$ instead of $\mathcal{O}(N^2)$ for a naive search.

2.3. Methodology of Instantaneous Reaction Simulation

A cursory look at Eq. (4) would suggest that instantaneous reactions ($k_f \to \infty$) would require $\Delta t \to 0$ to keep the probability less than unity. This is clearly impossible for the numerical method, so we seek an approximation. *Benson and Meerschaert* [29] showed that the coefficient k_f incorporates both the thermodynamic (well-mixed) rate and the volume associated with that rate. Perfect mixing (say, by stirring a beaker) eliminates concentration fluctuations by physical homogenization [59]. At some small volume in an un-stirred system, the point-wise law of mass action is assumed to be valid, and we may interpret this as the finite volume associated with a particle, with the rate k_f is tied to that volume. Therefore, we require that coincident particles ($s = 0$) will react with probability one for essentially instantaneous, or high-k_f reactions. In this case, plugging $\text{Prob}(react) = 1$ and $v(s = 0)$ into Eq. (4) leaves:

$$k_f(\Delta t)^{1/2} = N_0(24D)^{1/2}/(\Omega[B]_0). \tag{6}$$

All of the parameters on the right hand side are known; therefore, this equation gives a constraint on the combination of effective k_f and Δt that may be used to simulate an instantaneous reaction.

To determine whether a given reaction fits within this "instantaneous" criteria, we may check the Damkohler number, which compares the timescales of reaction relative to transport processes (e.g., dispersion, diffusion). *Dentz*

et al. [48] stated that the effective rate can be virtually any fraction of the local rate depending on the Damkohler number, and the conclusion is consistent with the fact that laboratory measured kinetic rates can be orders of magnitudes larger than their field measured counterparts (e.g., [60, 61]). The diffusive Damkohler number is a dimensionless ratio of diffusion time scale ($t_D = l^2/2D_m$) over reaction time scale ($t_r = 1/C_0k_f$) [59, 23, 21, 56], so that $D_a = t_D/t_r = C_0k_fl^2/2D_m$, where l is the size of concentration perturbations (e.g., [59, 23, 21]). The length l is typically taken as the size of a pore, but may be as large as the domain size [59, 6, 21]. If the Damkohler number is very large, the time scale of diffusion is much longer than that of the reaction and the reaction can be deemed as instantaneous. The D_a values range from 250 to 500 for *Raje and Kapoor's* experiments, and 9×10^5 to 5×10^8 in *Gramling et al.'s* experiments, assuming the length of l is the size of porous media particle [5]. Based on these numbers, we simulate the latter experiments with the instantaneous criteria defined by Eq. (6).

3. Results and Discussion

We simulated the two experiments by *Raje and Kapoor* [5] and three by *Gramling et al.* [12] by reproducing the two breakthrough curves (BTC) from the former and six concentration profiles from the latter. To help distinguish the experiments from the two groups, we use different symbols for the experimental results in the following plots. In addition, because there is randomness in the initial positions, movements, and reaction locations for the particles, each simulation will have some randomness in the particle densities at any time. To translate the particle numbers to concentrations for comparison to experiments, the particle numbers are counted at a length interval of approximately 0.5 cm (half the length of movement due to dispersion within a time step, $\sqrt{6D\Delta t}$) in each simulation. Then each PT simulation is run from 10 to 100 independent times to calculate the concentration ensemble means and standard deviations (error bars in the graphs). This procedure is similar to simulating conservative solutes with the PT method [54].

Figure 2 shows the PT simulations and measurements from *Raje and Kapoor's* [5] experiments. We use an initial number of particles in each simulation of $N_0 = 1000$ and a time step of $\Delta t = 1$ second. All other parameters are the same as those reported for the experiment, as shown in Table 1. The number of initial particles was not rigorously optimized, but rather chosen by visual fit. Concentration spatial covariance data was

not available to allow *a priori* estimation (see section 3.3). The agreement between the simulations and the data is quite good considering that the only parameter with any flexibility is the initial particle number N_0.

In our simulation of the experiments by *Gramling et al.* [12], the reaction is assumed to be instantaneous. Figures 3 and 4 illustrate simulation results and observations for two series of the experiments. The snapshots of the sand columns were taken in 2-D and the concentrations were averaged across the column to give a single concentration in the longitudinal (transport) direction. The first series (Fig. 3) is a sequence of snapshots of a single experiment run with a constant flow rate of 2.67 ml/min. The second series (Fig. 4) are single snapshots from three experiments conducted at different flow rates. Our simulations here differ only in that the time step sizes used (Δt =1, 0.1, and 0.01 seconds) correspond to the different flow rates (2.7 ml/min, 16 ml/min, and 150 ml/min, respectively). All time step lengths follow the time step rules described above in Eq. (6). For simulations, the initial particle number is $N_0 = 600$. The simulation of the instantaneous reaction and the *a priori* determination of particle numbers are discussed more specifically in Sections 3.2 and 3.3.

Most of the experimental data are very close to the simulated means and nearly all are within one standard deviation (Figs. 2, 3, and 4). One can also discern the over-prediction by the ADRE (1) in product production, because the analytic solution (2) has a peak concentration at all times of $C_P/C_0 = 0.5$ [12]. In addition, we reproduce the results of Figure 6a in *Gramling et al.* [12] depicting the cumulative mass of product formed in one experiment and simulated mass from the PT method, as well as the analytical solution of a well-mixed system (Fig. 5). The graphs of cumulative product mass in experiments at all three velocities look very similar. To be consistent with previous simulation work (e.g., [53], [49]), we only present the results for the flow rate of 2.7 mL/min. All of our simulated rates of accumulation of reaction product are in close agreement with the experimental measurements.

The variability of the simulated concentrations, reflected in the standard deviations, is directly linked to particle numbers and incomplete mixing. As the number of particles goes to infinity, concentration variability goes to zero and the simulated reaction is perfectly mixed [29]. As the number gets very small, all of the reactant mass is in a few particles that are unlikely to come together. For a reasonable number of particles, reactions occur preferentially at interfaces, leading to increased segregation and poorer mixing. Reactions can only progress by diffusion or dispersion to the interface. In these column

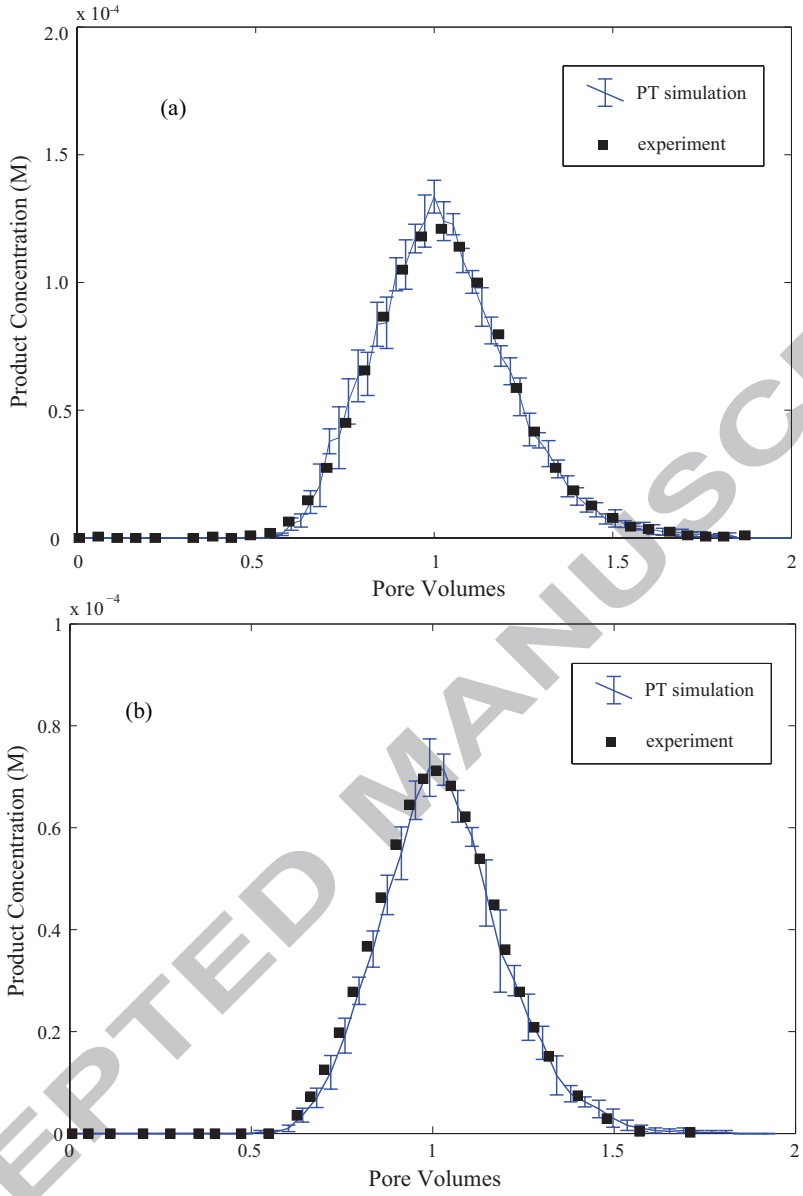

Figure 2: Simulations of product breakthrough curves from *Raje and Kapoor* [5]. Black squares are observations from the experiments, blue lines with error bars (mean values and plus/minus one standard deviation) are simulations using the PT method. a) Run 1: initial concentration of 0.5 mM, pore velocity = 0.096 cm/s. b) Run 2: initial concentration of 0.25 mM, pore velocity = 0.07 cm/s.

simulations, the fluctuations are thought to arise from non-uniformity in the pore-scale flow field [5]. Conceptually this is similar to a system where diffusion is the sole mode of transport [59], in which growing "islands" of reactants arise due to initial areas that have fluctuations in the initial reactant concentrations. The initial number of particles codes the spatial structure of the fluctuations and the decrease in particle numbers as a reaction progresses simultaneously leads to an increase in island size (chemical heterogeneity) and poorer levels of mixing.

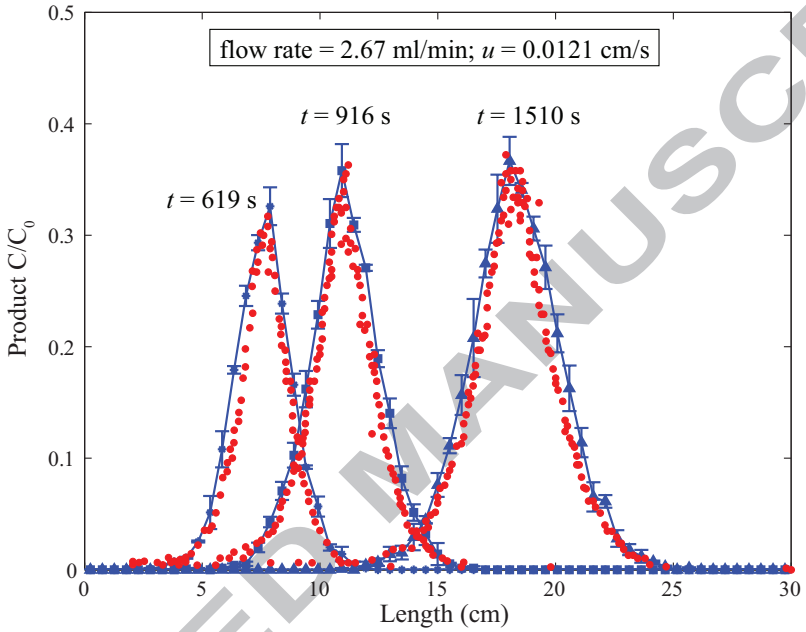

Figure 3: Simulations of the first series of experiments from *Gramling et al.* [12]: product concentration snapshots at different times. Red dots are measurements, blue lines with error bars are simulations using the PT method. The symbols (diamond, square, and triangle) are the mean values of one hundred runs, the error bars are the standard deviations of those runs.

3.1. Reaction Zone Tails

Besides the subdued peak product concentrations, another important finding from *Gramling et al.'s* [12] experiments is the larger reaction zone widths relative to the solution of the ADRE (1). In the concentration profiles (concentration vs. length), heavy leading and trailing edges are seen in

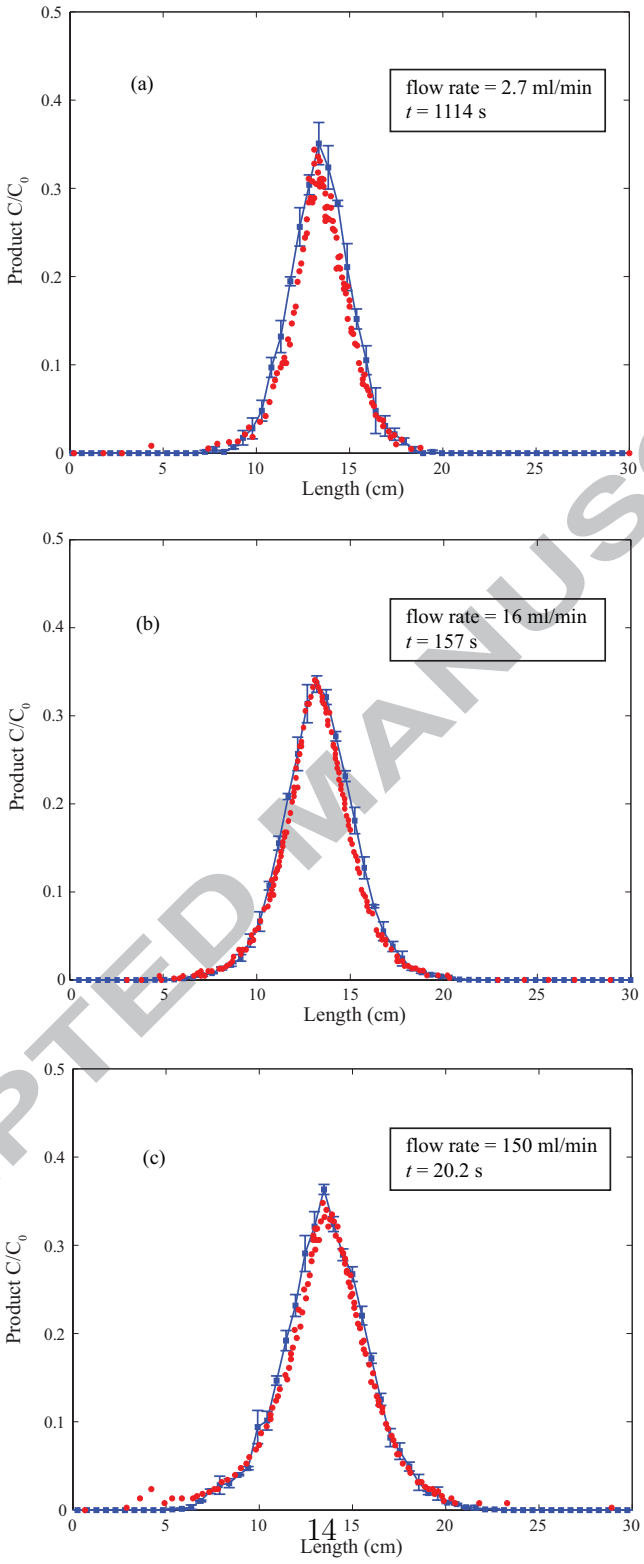

Figure 4: Simulations of the second series of experiments from *Gramling et al.* [12]: product concentration snapshots from experiments at different flow rates. Red dots are measurements, blue lines with error bars (mean values and standard deviations of ten runs) are simulations using the PT method. a) measurements at 1114 seconds at the flow rate of 2.7 ml/min; b) measurements at 157 seconds from experiments with flow rate of 16 ml/min; c) measurements at 20.23 seconds with a flow rate of 150 ml/min.

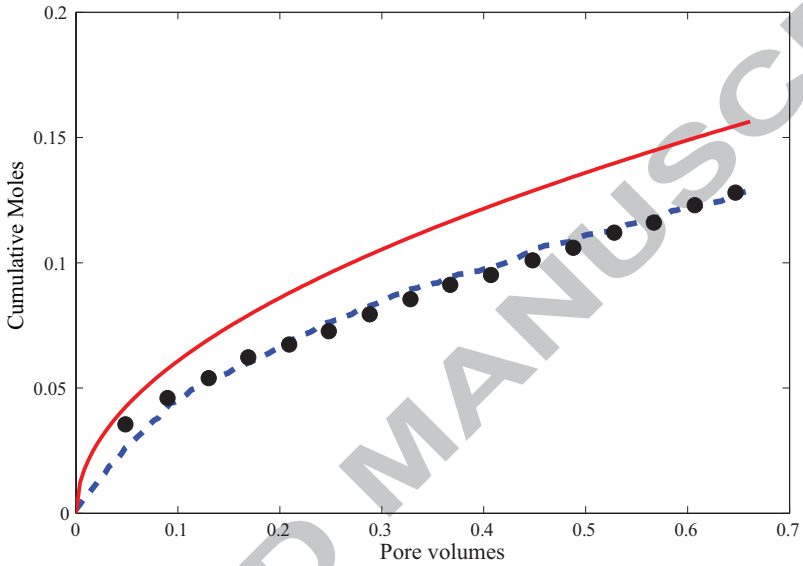

Figure 5: Total mass produced as a function of time for a flow rate of 2.7 mL/min in the *Gramling et al.* experiment [12]. The solid line represents the complete mixing theoretical model results, the points are measurements, and the dashed line denotes the results from our PT model.

the product concentration that are not evident in the analytic solution (see also [46]). A closer examination of this experiment and our PT simulations using a logarithmic concentration axis (Fig. 6) reveals greater measured product concentrations in both tails than the analytical solution (2), as well as the ability of the PT method to model this phenomenon.

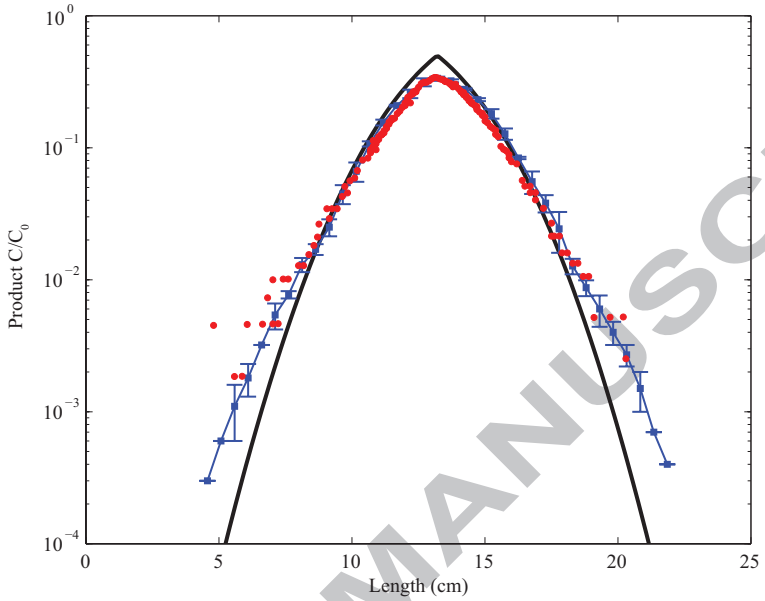

Figure 6: Semi-log plot of spatial concentration profiles from *Gramling et al.* [12]. Experimental measurements are red dots, PT simulations are blue lines through ensemble means, along with plus/minus one standard deviation, and the analytic solution of well-mixed ADRE (1) is plotted as black continuous line. These data are the same as shown in Figure 4b.

The product zone tails of these experiments already have generated some discussion. *Edery et al.* [20] reviewed models using a Fickian advection-dispersion equation (ADE) along with their PT reaction method based on an empirical effective radius of reaction [53], as well as the empirical kinetic reaction rate method used by *Sánchez-Vila et al.* [49], and concluded that these methods were unable to capture the forward and backward tails of the spatial concentration profiles. To overcome this issue, *Edery et al.* [20] used a continuous time random walk (CTRW) for the particle transport instead of the classical Brownian motion with the ADE governing equation. The time for each motion in CTRW is random and the heavier weights on the long-

time probability cause some particles to delay their migrations relative to the mean, hence there is a broader spread of both reactants and products. *Zhang and Papelis* [46] extended this concept by using both random times and non-Gaussian particle migration distances to match product concentration near the tails. Both of these approaches require several additional parameters. It is unclear if these methods, invoked to account for the tails in the reactive case, were calibrated from a conservative tracer, because simulations of the non-reactive tracer test were not displayed in [20] or [46]. The traditional (Fickian) ADE appears to match the conservative tracer quite well, i.e., a heavy trailing edge was not evident in the original analysis (see Fig. 1 and Figures 6 and 7 in the original [5]).

Luo and Cirpka [52] posited that material heterogeneity leads to the extended tailing behavior in breakthrough curves. Taking a similar view, the tails in the reaction product may be due to the reaction itself: if poor mixing or small-scale diffusion limits the reactions, then the reactants could venture farther into "enemy territory" before reacting, and the tails of the product distribution would be enlarged relative to the tails of well-mixed reaction. This is a significant and somewhat counter-intuitive finding. If heterogeneity was thought to (uniformly) reduce reaction rates, then the measured product concentrations would be everywhere lower than the well-mixed solution. This clearly is not the case. Our PT simulations give some insight into the heavier product tails. Conceptually, some A particles may move into the displaced B particles like fingers rather than a smooth, well-mixed front. The calculation of reaction based on local diffusion allows some probability of longer particle excursions, which is consistent with the conceptualization of *Cao and Kitanidis* [62], who showed that the slow rate of diffusion allows concentration gradients to be sustained at the small scale and a mass of reactant can cross the interface and interact with the other reactant only through diffusion.

3.2. Instantaneous Reactions

The reaction in *Gramling et al.'s* [12] experiments has a very high k_f and the Damkohler numbers are many orders-of-magnitude larger than unity given the range of possible correlation lengths. Here we use expression (6) to investigate the effect of different combinations of k_f and Δt (Fig. 7).

Various studies have provided quantitative criteria to classify a reaction as instantaneous. For instance, in a derivation of transport-controlled reaction rates, *Sánchez-Vila et al.* [63] showed that for a $D_a = 100$ or larger, the system reaches local equilibrium practically instantaneously, and results

using an approximation for the reaction rate are almost indistinguishable from those using an equilibrium reaction. From their point of view, to simulate the instantaneous reaction, the reaction rate constant can be arbitrarily chosen as long as the D_a is larger than 100. *Tartakovsky et al.* [21] reached a similar conclusion. They found that the deterministic solutions of the diffusion-reaction equation are all the same if $D_a > C_{v0}^{-1}$, where the initial coefficient of variation, $C_{v0} = \sigma_C/C_0 < 1$, where σ_C is the concentration standard deviation. For *Gramling et al.'s* [12] experiments, taking a conservative characteristic length value as the size of pore space, 0.13 cm, a value of reaction rate constant larger than $0.42M^{-1}s^{-1}$ satisfies the criterion of $D_a > 100$. We test this by using the reaction rate over an order of magnitude larger to satisfy instantaneous reaction "criteria" (Fig. 7). While there is residual effect of increasing the rate coefficient, it appears that the thermodynamic part of the probability is not the determining factor in these simulations. Similarly, *Edery et al.* [53] indicated that the reactions in the experiments of [12] were more controlled by concentration fluctuations than by reaction rate.

3.3. Particle Numbers

It may appear that the number of particles used to represent the reactants is a free parameter. However, *Benson and Meerschaert* [29] showed that the number of particles is directly related to the time of onset of reactant self-segregation and reduced reaction rates in simple diffusion systems. Using more particles means that the reactant concentrations are smoother functions of space, i.e., more perfectly mixed. We may test the sensitivity to this estimate by varying the numbers of particles while holding all other parameters constant in the simulation. Because of the similarity of the experiments, we present the simulation of the second experiment (flow rate of 16 mL/min) from [12] as an example. Three simulation runs are shown in Figure 8. When using one-tenth the number of particles to represent the reactants ($N_0 = 60$), the ratio of product concentration over initial concentration is only around 0.25; when using ten times more particles ($N_0 = 6,000$), the predicted product profile (C/C_0) is approximately 0.40. As the number of particles increases to infinity, the product profile would approach 0.5, which is the maximum value in a well-mixed system (i.e., the analytic solution to the 1D ADRE (2)). From this point of view, the PT model applied in this study is capable of simulating the incomplete mixing that is characterized by

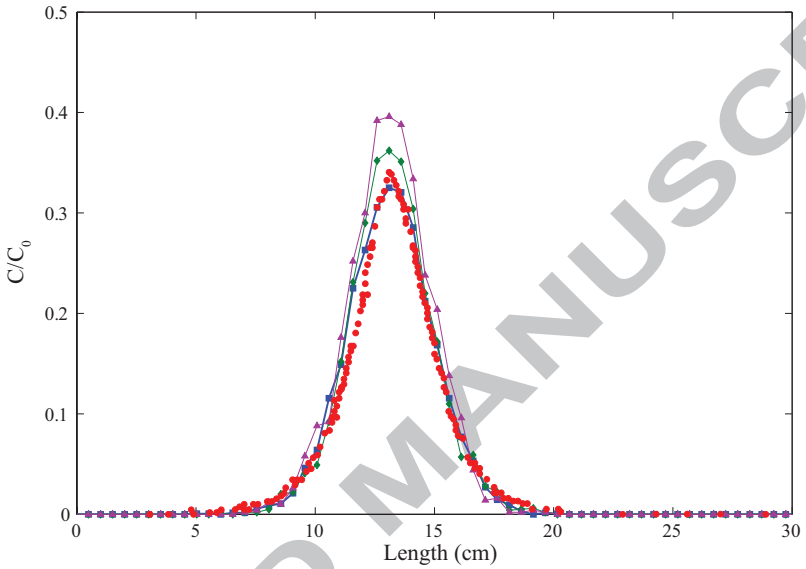

Figure 7: Simulations of instantaneous reaction using different combinations of reaction rates and time steps. Maintaining a maximum probability of reaction of unity in Eq. (6), we have k_f and Δt values, in units of $M^{-1}s^{-1}$ and s, respectively, of 4.08 and 1 (line with squares); 12.9 and 0.1 (line with diamonds), and 40.8 and 0.01 (line with triangles). The same experimental data shown in Figure 4b is reproduced here.

high variance and/or larger concentration fluctuations by choosing a suitable number of particles.

A recent study by *Bolster et al.* [59] enables a method to determine the number of particles that should be used to represent the reactants in the columns. Based on the continuum reaction equation, the authors showed that the pseudo-kinetic slowdown due to diffusion-limited mixing is directly proportional to the covariance of initial concentration perturbations, which they approximated with a Dirac delta function $\overline{C'_A(x,0)C'_A(y,0)} = \sigma_C^2 l^d \delta(x-y)$, where σ_C^2 is the early-time concentration variance and l^d is the d-dimensional correlation length representative of concentration perturbations. It has long been known for conservative solutes that the number of particles in a PT simulation is inversely proportional to the variance of concentration [64, 65]. Therefore, the numbers of particles representing the same amount of mass should, in part, dictate the rate of reactions. As a first approximation, *Paster et al.* [66, 45] considered each particle individually as a delta function of concentration, and showed that the covariance of the concentration, upon initiation of the simulation, is $\overline{C'_A(x,0)C'_A(y,0)} = (C_0^2\Omega/N_0)\delta(x-y)$. Equating the particle and continuum concentration covariance gives

$$N_0 = \frac{C_0^2\Omega}{\sigma_C^2 l^d}. \tag{7}$$

We can estimate the size and variance of concentration perturbations using the high-resolution snapshots given in Figure 3b of [12]. The original raw images of light transmission are no longer available [*C. Harvey, personal communication*] so we use the color images for $t = 619$ [s], which have integer values of red, green, and blue (RGB) saturations from 0 to 255. For a perfectly mixed experiment, any vertical transect of pixels would be the same color and have no variability in any color saturation. On the contrary, the measured vertical transects have systematic changes in the variance of the RGB components, from the lowest value far in front of the invading fluid (Fig. 9), to the greatest in the zone of equal reactant concentrations. Using the fact that $VAR(aX) = a^2 VAR(X)$ for a constant a and assuming for this estimate that the RGB variances are additive, then the variance of concentration in the mixing zone can be estimated. This assumption is best in those areas where one color dominates the color map. The range of concentration is on the order of 0 to 0.02 M, while color saturations are between 0 and 255, or $10^{4.1}$ greater. In the area of greatest concentration contrasts, the variance of color saturation is on the order of 2000 above background

noise (Fig. 9b), so that the variance of concentration is approximately on the order of $\sigma_C^2 \approx 2000/10^{8.2}\mathrm{M}^2$.

Furthermore, the color fluctuations have some coherent structure upon visual inspection (Fig. 9a) that can be deduced with a fast Fourier transform (FFT) (Fig. 9c). Each vertical column of pixel colors, upon FFT, has several frequencies that dominate, revealing some coherent structures. These (spatial) frequencies are typically in the range of 2 to 4 times the inverse of the column width of 50 pixels. Note that the mean value of each color, which is irrelevant here, is removed before each FFT so that the zero frequency value is zero. This has no effect on the other frequencies. We automated the identification of spatial structure in the column's transverse direction by selecting the single dominant frequency (in terms of power spectrum) for each vertical trace for each color and plotting those for the entire column length after conversion to wavelength (Fig. 10). It appears that the dominant frequencies have wavelengths between 25% to 100% of the column's 5.5 cm width (Fig. 10). This corresponds to fingers or "blobs" (half wavelength) of widths $l \approx 0.9$ to 2.5 cm. Using $l = 1.4$ cm (wavelength of 25 pixels, see Fig. 10) and plugging the other numbers into Eq. (7) gives an estimate of the number of particles of roughly 680, compared to the 600 we used to visually fit the reaction zones. This is a qualitative demonstration that the theoretical number of particles is consistent with the number we used. A more concrete estimate would require more detailed measurement of concentration variance and spatial correlation.

4. Conclusions and Recommendations

In this study, we implement a novel particle tracking method that calculates the probability that any two particles under general conditions of advection, dispersion, and diffusion occupy the same position. When combined with the thermodynamic probability manifested in the well-mixed rate coefficient, the combined effects of transport and mixing-limited reaction are accurately simulated. Simulation results are tested against breakthrough curves reported by *Raje and Kapoor* [5] and concentration profiles from *Gramling et al.* [12]. Not only do the simulation results match the cumulative and peak product concentrations, but also agree with the forward and backward tails of the reaction zone. The agreement between simulations and laboratory observations shows that this particle tracking method is able to successfully

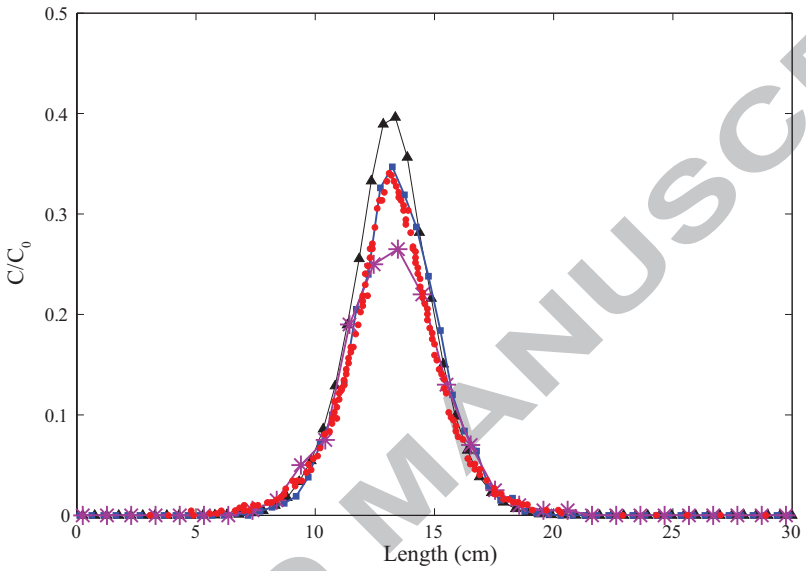

Figure 8: Effect of particle numbers, using the second experiments from [12] as a base case, shown as Figure 4b. For all runs simulating instantaneous reaction, using the higher number of particles ($N = 6,000$), the model predicted that the product concentration over initial reactant concentration was around 0.40, which over-predicts experimental observations (red dots). The simulation with the lower number of particles ($N = 60$) under-predicted the measurements, the ratio was around 0.25.

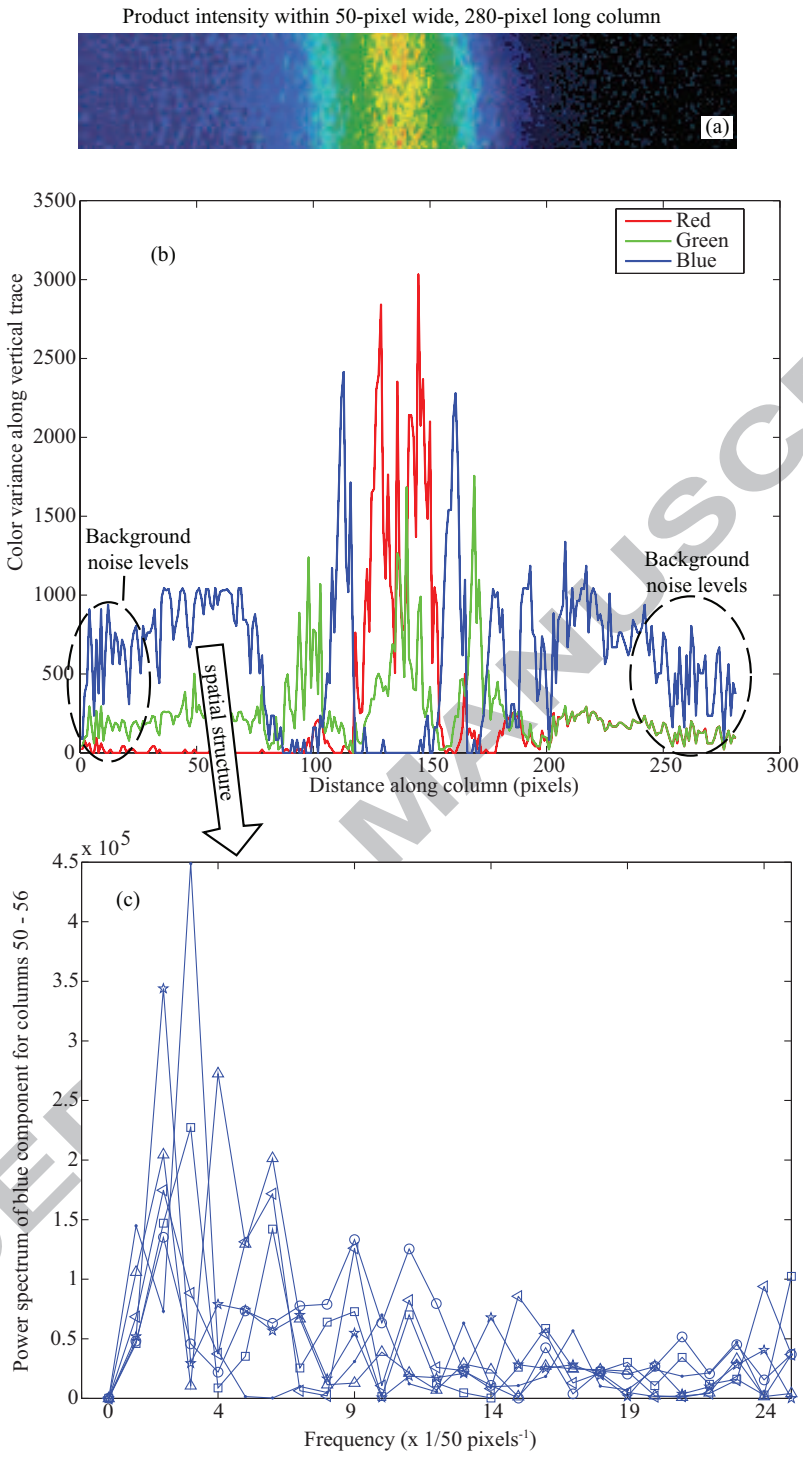

Figure 9: a) Example color map (after [12]) of product concentration at $t = 619$ s for flow rate $Q = 2.67$ mL/min; b) variance in red, green, and blue color components in vertical transects; c) example power spectrum of blue component in columns 50 through 56, showing dominant spatial frequencies of 2/50 to 4/50 pixels^{-1}.

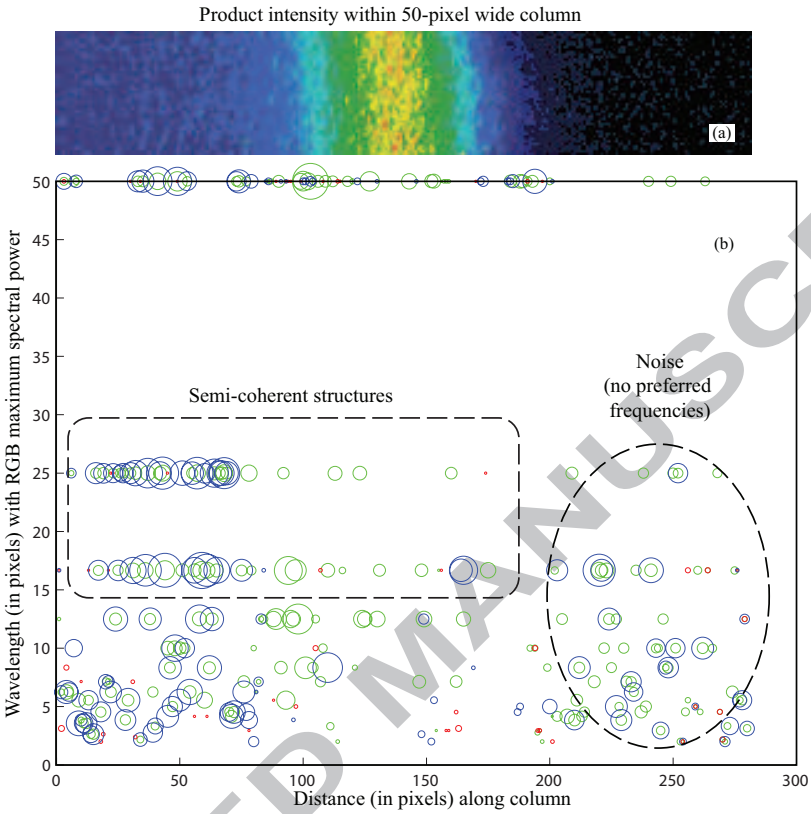

Figure 10: a) Example color map of reaction product concentrations (after [12]); b) dominant wavelength from the power spectrum for each color in every vertical transect. Circle color represents color component (R, G, or B) and size is proportional to spectral power at the dominant wavelength. A lack of systematic dominant wavelengths at the downstream (right) end of the column indicates uncorrelated noise.

simulate observations without invoking any additional parameters or coefficients.

The only flexible numerical parameter in our model, the number of particles, represents fluctuations in concentrations, i.e., the product of concentration (spatial) variance and correlation length. This information may be gained by direct measurement of the concentration field on either small [12] or large scales [67], or by stochastic means [68, 69, 70, 6]. Using visual data of transmitted light in the experiments of [12], we derived particle numbers that matched the best-fit numbers very closely; however, the estimate is likely to have fairly large variability, the magnitude of which we do not endeavor to quantify at this point.

The particle transport and reaction algorithm presented here has yet to be extended to more complex reaction chains. This is not a theoretical problem as reactions with multiple reactants or uneven stoichiometry as a series of two-particle interactions (see *Gillespie* [71]), though it may present numerical difficulties. The particle reaction algorithm also has not been coupled to detailed 3-*d* velocity fields for the purpose of validating, for example, *Molz and Widdowson's* [1] conjecture that poor mixing is primarily responsible for pseudo-kinetic reactions in heterogeneous flow fields at the field scale.

5. Acknowledgments

We thank Aaron Packman, Antoine Aubeneau, and five other anonymous reviewers for extremely thoughtful and helpful reviews. DAB was supported by NSF grant EAR–0749035, and USDOE Basic Energy Sciences grant DE-FG02-07ER15841. DB and AP were supported by NSF grant EAR-1113704. Any opinions, findings, conclusions, or recommendations do not necessary reflect the views of the NSF or DOE.

References

[1] F. J. Molz, M. A. Widdowson, Internal inconsistencies in dispersion-dominated models that incorporate chemical and microbial kinetics, Water Resour. Res. 24 (4) (1988) 615–619.

[2] L. Li, C. A. Peters, M. A. Celia, Upscaling geochemical reaction rates using pore-scale network modeling, Advances in Water Resources 29 (9) (2006) 1351–1370.

[3] C. I. Steefel, D. J. DePaolo, P. C. Lichtner, Reactive transport modeling: An essential tool and a new research approach for the earth sciences, Earth and Planetary Science Letters 240 (34) (2005) 539–558.

[4] D. M. Tartakovsky, M. Dentz, P. C. Lichtner, Probability density functions for advective-reactive transport in porous media with uncertain reaction rates, Water Resour. Res. 45 (2009) W07414.

[5] D. Raje, V. Kapoor, Experimental study of bimolecular reaction kinetics in porous media, Environ. Sci. Technol 34 (2000) 1234–1239.

[6] M. Dentz, T. L. Borgne, A. Englert, B. Bijeljic, Mixing, spreading and reaction in heterogeneous media: a brief review, Journal of Contaminant Hydrology 120-121 (2011) 1–17.

[7] J. Luo, M. Dentz, J. Carrera, P. K. Kitanidis, Effective reaction parameters for mixing controlled reactions in heterogeneous media, Water Resour. Res. 44 (2008) W02416, 12 pp.

[8] V. Kapoor, L. W. Gelhar, F. Miralles-Wilhelm, Bimolecular second-order reactions in spatially varying flows: Segregation induced scale-dependent transformation rates, Water Resour. Res. 33 (4) (1997) 527–536.

[9] D. Bolster, D. A. Benson, T. L. Borgne, M. Dentz, Anomalous mixing and reaction induced by superdiffusive nonlocal transport, Phys. Rev. E 82 (2010) 02119.

[10] A. M. Tartakovsky, D. M. Tartakovsky, P. Meakin, Stochastic langevin model for flow and transport in porous media, Phys. Rev. Lett. 101 (2008) 044502.

[11] A. Tartakovsky, G. Tartakovsky, T. Scheibe, Effects of incomplete mixing on multicomponent reactive transport, Advances in Water Resources 32 (11) (2009) 1674 – 1679.

[12] C. Gramling, C. F. Harvey, L. C. Meigs, Reactive transport in porous media: A comparison of model prediction with laboratory visualization, Environ. Sci. Technol. 36 (2002) 2508–2514.

[13] D. Ding, Transport of bacteria in aquifer sediment: experiments and modeling, Hydrogeology Journal 18 (3) (2010) 669–679.

[14] M. Dentz, J. Carrera, Mixing and spreading in stratified flow, Physics of Fluids 19 (2006) 017107.

[15] P. K. Kitanidis, Particle-tracking equations for the solution of the advection-dispersion equation with variable coefficients, Water Resour. Res. 30 (11) (1994) 3225–3227.

[16] T. Le Borgne, M. Dentz, D. Bolster, J. Carrera, J. de Dreuzy, P. Davy, Non–Fickian mixing: Temporal evolution of the scalar dissipation rate in heterogeneous porous media, Adv. Water Res. 33 (12) (2010) 1468–1475.

[17] T. Le Borgne, M. Dentz, P. Davy, D. Bolster, J. Carrera, J.-R. de Dreuzy, O. Bour, Persistence of incomplete mixing: A key to anomalous transport, Phys. Rev. E 84 (1) (2011) 015301–. doi:10.1103/PhysRevE.84.015301.

[18] D. Bolster, F. J. Valds-Parada, T. LeBorgne, M. Dentz, J. Carrera, Mixing in confined stratified aquifers, Journal of Contaminant Hydrology 120–121 (0) (2011) 198–212. doi:10.1016/j.jconhyd.2010.02.003.

[19] O. A. Cirpka, P. K. Kitanidis, Characterization of mixing and dilution in heterogeneous aquifers by means of local temporal moments, Water Resour. Res. 36 (5) (2000) 1221–1236.

[20] Y. Edery, A. Guadagnini, H. Scher, B. Berkowitz, Reactive transport in disordered media: role of fluctuations in interpretation of laboratory experiment, Adv. Water Resour. In press, http://dx.doi.org/10.1016/j.advwatres.2011.12.008,.

[21] A. M. Tartakovsky, P. de Anna, T. Le Borgne, A. Balter, D. Bolster, Effect of spatial concentration fluctuations on effective kinetics in diffusion-reaction systems, Water Resour. Res. 48 (2) (2012) W02526–.

[22] O. A. Cirpka, P. K. Kitanidis, An advective-dispersive stream tube approach for the transfer of conservative-tracer data to reactive transport, Water Resour. Res. 36 (5) (2000) 1209–1220.

[23] C. Knutson, A. Valocchi, C. Werth, Comparison of continuum and pore-scale models of nutrient biodegradation under transverse mixing conditions, Advances in Water Resources 30 (2007) 1421 – 1431.

[24] O. A. Cirpka, E. O. Frind, R. Helmig, Numerical simulation of biodegradation controlled by transverse mixing, Journal of Contaminant Hydrology 40 (2) (1999) 159 – 182.

[25] P. Danckwerts, Continuous flow systems: Distribution of residence times, Chemical Engineering Science 2 (1) (1953) 1–13. doi:10.1016/0009-2509(53)80001-1.

[26] E. Nauman, B. Buffham, Mixing in continuous flow systems, Wiley, 1983.

[27] J. C. Hill, Homogeneous turbulent mixing with chemical reaction, Annual Review of Fluid Mechanics 8 (1976) 135–161.

[28] A. Lehwald, G. Janiga, D. Thvenin, K. Zhringer, Simultaneous investigation of macro- and micro-mixing in a static mixer, Chemical Engineering Science 79 (0) (2012) 8–18. doi:10.1016/j.ces.2012.05.026.

[29] D. A. Benson, M. M. Meerschaert, Simulation of chemical reaction via particle tracking: Diffusion-limited versus thermodynamic rate-limited regimes, Water Resour. Res. 44 (2008) W12201.

[30] D. R. LeBlanc, S. P. Garabedian, K. M. Hess, L. W. Gelhar, R. D. Quadri, K. G. Stollenwerk, W. W. Wood, Large-scale natural gradient tracer test in sand and gravel, cape cod, massachusetts: 1. experimental design and observed tracer movement, Water Resour. Res. 27 (5) (1991) 895–910.

[31] Q. Kang, P. C. Lichtner, D. Zhang, An improved lattice boltzmann model for multicomponent reactive transport in porous media at the pore scale, Water Resour. Res. 43 (12) (2007) W12S14–.

[32] X. Sánchez-Vila, L. D. Donado, A. Guadagnini, J. Carrera, A solution for multicomponent reactive transport under equilibrium and kinetic reactions, Water Resour. Res. 46 (7) (2010) W07539–.

[33] A. M. Tartakovsky, P. Meakin, T. D. Scheibe, B. D. Wood, A smoothed particle hydrodynamics model for reactive transport and mineral precipitation in porous and fractured porous media, Water Resour. Res. 43 (5) (2007) W05437–.

[34] P. deAnna, T. LeBorgne, M. Dentz, D. Bolster, P. Davy, Anomalous kinetics in diffusion limited reactions linked to non-gaussian concentration probability distribution function, Journal of Chemical Physics 135 (2011) 174104.

[35] A. M. Tartakovsky, G. Redden, P. C. Lichtner, T. D. Scheibe, P. Meakin, Mixing-induced precipitation: Experimental study and multiscale numerical analysis, Water Resour. Res. 44 (6) (2008) W06S04–.

[36] D. Ronen, M. Magaritz, H. Gvirtzman, W. Garner, Microscale chemical heterogeneity in groundwater, Journal of Hydrology 92 (12) (1987) 173–178.

[37] R. L. Smith, R. W. Harvey, D. R. LeBlanc, Importance of closely spaced vertical sampling in delineating chemical and microbiological gradients in groundwater studies, Journal of Contaminant Hydrology 7 (3) (1991) 285 – 300.

[38] J. A. Davis, D. B. Kent, J. A. Coston, K. M. Hess, J. L. Joye, Multispecies reactive tracer test in an aquifer with spatially variable chemical conditions, Water Resour. Res. 36 (2000) 119–134.

[39] K. Mayer, S. Benner, E. Frind, S. Thornton, D. Lerner, Reactive transport modeling of processes controlling the distribution and natural attenuation of phenolic compounds in a deep sandstone aquifer, Journal of Contaminant Hydrology 53 (34) (2001) 341–368.

[40] K. U. Mayer, E. O. Frind, D. W. Blowes, Multicomponent reactive transport modeling in variably saturated porous media using a generalized formulation for kinetically controlled reactions, Water Resour. Res. 38 (9) (2002) 1174–.

[41] P. A. Herrera, M. Massab, R. D. Beckie, A meshless method to simulate solute transport in heterogeneous porous media, Advances in Water Resources 32 (3) (2009) 413 – 429.

[42] A. M. Tartakovsky, P. Meakin, Pore scale modeling of immiscible and miscible fluid flows using smoothed particle hydrodynamics, Advances in Water Resources 29 (10) (2006) 1464 – 1478.

[43] D. T. Gillespie, A general method for numerically simulating the stochastic time evolution of coupled chemical reactions, Journal of Computational Physics 22 (4) (1976) 403 – 434.

[44] D. T. Gillespie, The chemical langevin equation, J. Chem. Phys. 113 (2000) 297–306.

[45] A. Paster, D. Bolster, D. A. Benson, Particle tracking and the diffusion-reaction equation, Water Resour. Res. – (submitted) –.

[46] Y. Zhang, C. Papelis, Particle-tracking simulation of fractional diffusion-reaction processes, Phys. Rev. E 84 (2011) 066704.

[47] Y. Edery, H. Scher, B. Berkowitz, Modeling bimolecular reactions and transport in porous media, Geophys. Res. Lett. 36 (2009) L02407.

[48] M. Dentz, P. Gouze, J. Carrera, Effective non-local reaction kinetics for transport in physically and chemically heterogeneous media, Journal of Contaminant Hydrology 120-121 (0) (2011) 222 – 236.

[49] X. Sánchez-Vila, D. Fernàndez-Garcia, A. Guadagnini, Interpretation of column experiments of transport of solutes undergoing an irreversible bimolecular reaction using a continuum approximation, Water Resour. Res. 46 (2010) W12510.

[50] L. D. Donado, X. Sánchez-Vila, M. Dentz, J. Carrera, D. Bolster, Multicomponent reactive transport in multicontinuum media, Water Resour. Res. 45 (11) (2009) W11402–.

[51] M. Willmann, J. Carrera, X. Sánchez-Vila, M. D. O. Silva, Coupling of mass transfer and reactive transport for nonlinear reactions in heterogeneous media, Water Resour. Res. 46 (2010) W07512, 15 PP.

[52] J. Luo, O. A. Cirpka, How well do mean breakthrough curves predict mixing-controlled reactive transport, Water Resour. Res. 47 (2011) W02520, 12pp.

[53] Y. Edery, H. Scher, B. Berkowitz, Particle tracking model of bimolecular reactive transport in porous media, Water Resour. Res. 46 (2010) W07524.

[54] E. M. LaBolle, G. E. Fogg, A. F. B. Tompson, Random-walk simulation of transport in heterogeneous porous media: Local mass-conservation problem and implementation methods, Water Resour. Res. 32 (3) (1996) 583–593.

[55] E. M. LaBolle, J. Quastel, G. E. Fogg, Diffusion theory for transport in porous media: Transition-probability densities of diffusion processes corresponding to advection-dispersion equations, Water Resour. Res. 34 (7) (1998) 1685–1693.

[56] G. M. Porta, J.-F. Thovert, M. Riva, A. Guadagnini, P. M. Adler, Microscale simulation and numerical upscaling of a reactive flow in a plane channel, Phys. Rev. E 86 (3) (2012) 036102–.

[57] J. L. Bentley, Multidimensional binary search trees used for associative searching, Communications of the ACM 18 (1975) 509–517.

[58] A. Tagliasacchi, Matlab kd-tree library (9 2010).

[59] D. Bolster, P. de Anna, D. A. Benson, A. M. Tartakovsky, Incomplete mixing and reactions with fractional dispersion, Advances in Water Resources 37 (0) (2012) 86 – 93.

[60] A. F. White, S. L. Brantley, The effect of time on the weathering of silicate minerals: why do weathering rates differ in the laboratory and field?, Chemical Geology 202 (34) (2003) 479–506.

[61] L. Li, C. I. Steefel, L. Yang, Scale dependence of mineral dissolution rates within single pores and fractures, Geochimica et Cosmochimica Acta 72 (2008) 360–377.

[62] J. Cao, P. K. Kitanidis, Pore-scale dilution of conservative solutes: An example, Water Resour. Res. 34(8) (1998) 1941–1949.

[63] X. Sánchez-Vila, M. Dentz, L. D. Donado, Transport-controlled reaction rates under local non-equilibrium conditions, Geophys. Res. Lett. 34 (10) (2007) L10404–.

[64] E. M. LaBolle, J. Quastel, G. E. Fogg, J. Gravner, Diffusion processes in composite porous media and their numerical integration by random walks: Generalized stochastic differential equations with discontinuous coefficients, Water Resour. Res. 36 (3) (2000) 651–662.

[65] P. Chakraborty, M. M. Meerschaert, C. Y. Lim, Parameter estimation for fractional transport: A particle-tracking approach, Water Resour. Res. 45 (10) (2009) W10415–.

[66] A. Paster, D. Bolster, D. A. Benson, Connecting the dots: application of a particle method to the diffusion-reaction equation, Advances in Water Resources – (submitted) –.

[67] L. W. Gelhar, C. Welty, K. R. Rehfeldt, A critical review of data on field-scale dispersion in aquifers, Water Resour. Res. 28 (7) (1992) 1955–1974.

[68] A. Fiori, G. Dagan, Concentration fluctuations in transport by groundwater: Comparison between theory and field experiments, Water Resour. Res. 35 (1) (1999) 105–112.

[69] A. Fiori, S. Berglund, V. Cvetkovic, G. Dagan, A first-order analysis of solute flux statistics in aquifers: The combined effect of pore-scale dispersion, sampling, and linear sorption kinetics, Water Resour. Res. 38 (8) (2002) 1137–.

[70] A. Fiori, F. Boso, F. P. J. de Barros, S. De Bartolo, A. Frampton, G. Severino, S. Suweis, G. Dagan, An indirect assessment on the impact of connectivity of conductivity classes upon longitudinal asymptotic macrodispersivity, Water Resour. Res. 46 (8) (2010) W08601–.

[71] D. T. Gillespie, Exact stochastic simulation of coupled chemical reactions, J. Phys. Chem. 81 (25) (1977) 2340–2361.

Highlights for manuscript:" Modeling Bimolecular Reactions and Transport in Porous Media Via Particle Tracking"

Application of Lagrangian particle tracking model to reactive transport
No empirical parameters or assumptions in simulation
Accurate simulation of physical experiments on Diffusion controlled, mixing-limited reaction